The underlying degradation mechanisms of typical organophosphorus flame retardants in water based on identified intermediates and C, H and O isotope fractionation

Jukun Xiong [a,b], Yi Guo [a,b], Suyun Chen [a,b], Zicong Wang [a,b], Guiying Li [a,b], Faina Gelman [c], Meicheng Wen [a,b], Yanpeng Gao [a,b], Taicheng An [a,b,*]

[a] *Guangdong Key Laboratory of Environmental Catalysis and Health Risk Control, Guangdong-Hong Kong-Macao Joint Laboratory for Contaminants Exposure and Health, Institute of Environmental Health and Pollution Control, Guangdong University of Technology, Guangzhou 510006, China*
[b] *Guangdong Basic Research Center of Excellence for Ecological Security and Green Development, Guangdong Technology Research Center for Photocatalytic Technology Integration and Equipment Engineering, School of Environmental Science and Engineering, Guangdong University of Technology, Guangzhou 510006, China*
[c] *Geological Survey of Israel, 32 Yeshayauhu Leibowitz Street, Jerusalem 9692100, Israel*

ARTICLE INFO

ABSTRACT

Compound-specific stable isotope analysis (CSIA) is an innovative tool for tracing degradation mechanisms of organic pollutants in environments. Application of CSIA to characterize UV/H_2O_2 degradation processes of organophosphorus flame retardants (OPFRs), however, has hardly been explored. In this study, the underlying reaction mechanisms of typical OPFRs - tris(1-chloro-2-propyl) phosphate (TCPP) under UV/H_2O_2 condition have been explored. Special attention was given to multi-element (C, H and O) isotope fractionation during UV/H_2O_2 degradation. Results showed that TCPP was rapidly degraded in UV/H_2O_2 system with hydroxyl radical ($^\bullet$OH) as the main reactive species (ROSs), leading to a significant oxygen isotope fractionation ($\Delta\delta^{18}O = -2.98$ ‰, $\varepsilon_O = +2.6 \pm 0.5$ ‰). Furthermore, phosphorus-oxygen (P-O) bond cleavage was found to be the rate-limiting step through the density functional theory (DFT) calculations. No observable hydrogen isotope fractionation and remarkable carbon isotope fractionation ($\Delta\delta^{13}C = 1.50$ ‰, $\varepsilon_C = -1.9 \pm 0.4$ ‰) indicated that carbon-chlorine (C-Cl) bond rather than carbon-hydrogen (C-H) bond cleavage was a rate-limiting step. Multi-element CSIA revealed that the UV/H_2O_2 degradation of TCPP initiated by the breaking of P-O and C-Cl bonds. Our study emphasizes the prospect of combining multi-element CSIA with DFT calculations for a better evaluation of underlying mechanisms within the fate of TCPP in environments.

1. Introduction

Organophosphorus flame retardants (OPFRs) are flame retardants extensively used in commercial and building products, including plastics, fabrics, electronics, floor polishes, hydraulic fluids, and construction materials [1,2]. Tris(1-chloro-2-propyl) phosphate (TCPP), one of the typical OPFRs, is registered as a high production volume chemical under Registration, Evaluation, Authorization, and Restriction of Chemicals (REACH) of $10,000 - 100,000$ tons per year [3] and is the most important OPFRs [4]. Several studies reported that TCPP has been frequently detected in surface waters, sludges, soils, sediments, and even human due to the leakage from various products into environments [5–7]. Since TCPP is known as emerging pollutant with neurotoxic,

carcinogenic, and reprotoxic properties [8,9], it has been included in the European Commission priority list [10]. Furthermore, after TCPP enters the environments, it will undergo various degradation, leading to the significant changes including the concentration, structure, persistence, toxicity, bioaccumulation, and potential risks. Therefore, it is significant to investigate its degradation mechanisms in environments.

Photodegradation reactions are the important abiotic degradation pathways of TCPP in environments. Previous studies have proven that TCPP can be transformed by ultraviolet and sunlight irradiation under different condition [11–14]. In addition, Antonopoulou et al. [15] find that the main structural alteration of TCPP occurs in the chlorinated isopropyl group (-C_3H_5Cl) and the loss of one chlorinated isopropyl group (-C_3H_5Cl) lead to the formation of bis(1-chloro-2-propyl)

phosphate during TiO$_2$ photocatalysis of TCPP. Yu et al. [16] propose that the central phosphate, C-Cl bond and methyl group may be attacked by hydroxyl radicals ($^\bullet$OH) and bis(1-chloro-2-propyl) phosphate is formed through the loss of chlorinated isopropyl group (-C$_3$H$_5$Cl) from the central phosphorus of TCPP during UV/TiO$_2$ photocatalysis. Further, they perform the TCPP degradation under UV/H$_2$O$_2$ condition and find the central phosphorus of phosphate triester being first attacked by $^\bullet$OH, followed by breaking one oxygen-chlorinated isopropyl group (-O-C$_3$H$_5$Cl) to generate bis(1-chloro-2-propyl) phosphate [13]. He et al. [12] report that UV/H$_2$O$_2$ can lead the degradation of TCPP into dechlorinated and hydroxylated intermediates. Son et al. [17] find that the main degradation pathway of TCPP in the UV/H$_2$O$_2$ reaction system is the hydroxylation by $^\bullet$OH. Collectively, these previous studies propose three possible degradation pathways for TCPP in environments, including substitution of -C$_3$H$_5$Cl or -O-C$_3$H$_5$Cl moieties by $^\bullet$OH, substitution of chlorine atom by cleavage of C-Cl bond on -C$_3$H$_5$Cl moieties, or H abstraction from methyl group. Despite the fact that TCPP degradation has been widely explored and possible degradation pathways are proposed based on identification of transformation intermediates, the reaction mechanisms of TCPP in environments are not fully understood due to the lack of the confirmed evidences.

Compound-specific stable isotope analysis (CSIA) is an innovative method for tracing underlying reaction mechanisms of organic pollutants, even if competing reaction pathways occur and reaction products are partially unknown [18–20]. Isotope fractionation observed in individual organic compound can often be attributed to changes in bonds during the reaction and is thus a valuable indicator for identifying the type of reaction that initiates pollutant degradation [21,22]. Changes in bonds, especially bond-breaking reactions in the rate-limiting step, are typically considered the primary source of isotope fractionation [23,24]. Wu et al. [25] investigate the carbon isotope fractionation of hydrolysis and photolysis of the extensively used organophosphorus pesticides and find that carbon isotope fractionation can be used to characterize hydrolysis reaction and direct photolysis in environments. Further, the same group [26] investigates isotopic fractionation patterns of organophosphorus compounds during hydrolysis, photolysis and radicals oxidation processes, and finds that hydrogen and carbon isotope fractionation can be used diagnostically to characterize degradation pathways of phosphates, phosphorothioates and phosphorodithioates. Liu et al. [27] use tributyl phosphate as a model compound of trialkyl substituted organophosphate esters to determine carbon and hydrogen isotope fractionation associated with bond-breaking reactions under UV/H$_2$O$_2$ oxidation. They find that dual isotope analysis has diagnostic value for characterizing the chemical transformation of tributyl phosphate in environments. Although isotope fractionation patterns have been used to characterize the reaction mechanisms in many studies, little is known about isotopic fractionation of TCPP under UV/H$_2$O$_2$ photodegradation. Therefore, the isotope effects may be very informative for elucidation of UV/H$_2$O$_2$ degradation pathways.

Due to UV/H$_2$O$_2$ degradation is a very important pathway of organophosphorus compounds in the environments, data on isotope effects associated with this transformation can be very helpful for characterizing the underlying reaction mechanisms of the degradation. In this study, we applied this novel approach of CSIA to explore C, H and O isotope fractionation patterns and isotope effects during UV/H$_2$O$_2$ degradation of TCPP in aquatic solution, and tried to find a relationship between the measured isotope fractionations of multi-element (C, H, O) and the important UV/H$_2$O$_2$ transformation pathways as well as the underlying reaction mechanisms. Moreover, the density-functional theory (DFT) calculations were also used to insight into underlying reaction mechanisms and isotopic elementary reactions of TCPP degradation. This study could be helpful in better understanding the significant underlying transformation mechanisms in laboratory studies and contaminated field sites.

2. Material and methods

2.1. Chemicals

Tris(1-chloro-2-propyl) phosphate (TCPP, CAS: 13674–84–5, $\geq$ 99.0 %) was obtained from ANPEL Laboratory Technologies (Shanghai) Inc. 2,2,6,6-Tetramethyl-4-hydroxy-piperidinyloxy (TMPD, CAS: 768–66–1, $\geq$ 99.0 %) and 5,5-dimethyl-1-pyrroline N-oxide (DMPO, CAS: 3317–61–1, $\geq$ 99.0 %) were used to trap reactive oxygen species (ROSs). GC grade of dichloromethane and hexane were purchased from Merck (Germany). GC grade of methanol (MeOH) and tert-butanol (TBA) were purchased from ANPEL scientific instrument Co., Ltd, China·H$_2$O$_2$, acetone and all other chemicals were at least reagent grade purchased from Guangzhou chemical reagent Co., Inc., China. Deionized water (18.2 MΩ/cm) to prepare the solution was generated by a milli-Q integral system (Merck & Co., Inc., Kenilworth, NJ, USA).

2.2. UV/H$_2$O$_2$ degradation experiments

The UV/H$_2$O$_2$ degradation of TCPP was conducted in a Pyrex reactor [28] with a high-pressure mercury lamp (300 W, 200 $\leq \lambda \leq$ 800 nm) as a light source and each experiment was performed in triplicate. The quartz tube reactors with volume of 50 mL (diameter: 2.4 cm, height: 2.0 cm) were used throughout in these experiments and the temperature was kept at 25 °C $\pm$ 1 °C. The concentrations of TCPP and H$_2$O$_2$ were 1.0 and 0.5 mg/L, respectively, without specific mention of concentrations. The pH value was maintained at 8.0 with phosphate buffer (0.014 mol/L). Total 1.0 mL reaction solution was sampled at required interval for further qualitative and quantitative analysis.

2.3. Quenching experiments and EPR analysis

The scavenging experiments were performed using TBA (10 mM) and MeOH (10 mM) to quench $^\bullet$OH. Further, to detect the radicals involved in the UV/H$_2$O$_2$ degradation of TCPP, electron parameter resonance (EPR) spectra were recorded using a Bruker EMX Plus-10/12 spectrometer (Bremen, Germany), operated at 20 mW microwave power (9.85 GHz) with 100 G sweep width and 100 kHz modulation frequency. The center field was set as 3510 G. Samples (50 μL) were placed in quartz flat cell of total capacity 50 μL and irradiated directly inside the microwave cavity of the spectrometer using a 1 kW Xe arc lamp. Radiation from the lamp was passed through a 30 mm pathlength liquid filter (λ > 400 nm; aqueous solution containing in g/L: NaNO$_2$ 48.4, Na$_2$CO$_3$ 1.0, and K$_2$CrO$_4$ 0.2) to remove wavelengths below 400 nm. Hyperfine coupling constants were obtained by accumulating, simulating and optimizing spectra on an IBM PC computer using software described elsewhere [29]. The accuracy of the coupling constant measurement was $\pm$ 0.02 G. Fremy's salt was used as a standard for determination of the EPR spectral g-values. TMPD was used as spin trap for singlet superoxide (O$_2^{\bullet-}$), while DMPO was employed to trap $^\bullet$OH [30]. The time between reaction initiation and onset of EPR scanning was controlled to less than 80 s.

2.4. HPLC/MS/MS analysis

An Agilent 6470 electrospray triple quadrupole mass spectrometer (ESI-MS/MS), coupled with an Agilent 1260 series high-performance liquid chromatograph (HPLC) system was used for quantification of TCPP. Chromatographic separation was conducted by a RRHD Eclipse Plus 95 A C18 column (100 × 2.1 mm, 1.8 μm; Agilent Technologies Inc.). The mobile phase was composed of 70 % methanol and 30 % milli-Q water (70:30, v/v) at a flow rate of 0.3 mL/min. The sample injection volume was 10 μL, and the column temperature was maintained at 40 °C. An electrospray interface (ESI) was used for MS/MS detection in positive ion mode at multiple reaction monitoring (MRM), and the MRM transition monitored was 329.0 > 99.0 for TCPP. N$_2$ was used as both

curtain and collision gas. Fragmentor was set as 100 V, the collision energy was 20 V, and cell accelerator voltage was 5 V. Capillary voltage was kept at 3000 kV.

2.5. UPLC-Q exactive orbitrap-HRMS analysis

TCPP and its degradation intermediates were identified by a Dionex U3000 ultra performance liquid chromatograph (UPLC) system (Thermo Scientific™, Bremen, Germany) coupled with a Q-exactive orbitrap high resolution mass spectrometer (Thermo Scientific™, Bremen, Germany). Chromatographic separation was achieved on a C18 column (100 × 2.1 mm, 1.9 μm) with 0.1 % formic acid in water (mobile phase A) and methanol (mobile phase B). The column temperature was maintained at 35 °C. A gradient elution at 0.25 mL/min flow rate was used as follows: started at 10 % B, increased to 90 % B over 30 min, held for 5 min; then decreased to 10 % B over 5 min, held for 3 min; maintained constant for a total run time of 43 min. The injection volume was 5 μL. More detailed information is available in Supporting Information (SI).

2.6. GC/IRMS analysis

Carbon isotope ratio analyses were carried out on a gas chromatograph to interface with combustion furnace connected with an isotope ratio mass spectrometry (GC/C/IRMS) system as described previously [30]. Briefly, samples (in hexane) were injected with a split ratio of 1:10 into a split injector at 250 °C with a flow rate of 1.2 mL/min. The separation was performed with a 7890B GC (Agilent Technologies Inc.) equipped with a HP-5 capillary column (30 m × 0.25 mm, 0.25 μm). The temperature program of GC oven was as follows: 80 °C for 1 min, ramped to 140 °C by 20 °C/min, held for 2 min, then ramped to 280 °C by 5 °C/min and held for 6 min. More detailed information about isotope analysis is available in SI.

Hydrogen isotope ratio analyses were carried out on a GC to interface with chromium-based high temperature conversion connected with isotope ratio mass spectrometry (GC/Cr-HTC/IRMS) [31,32]. Briefly, samples (in hexane) were injected to the GC via splitless in amounts that represented the hydrogen equivalent of ~150 nmol H on column with a flow rate of 1.2 mL/min. The temperature of injector was set at 250 °C. The parameters of GC were the same as the settings for carbon isotope ratio analyses.

Oxygen isotope ratio analyses were carried out on a gas chromatograph/pyrolysis/isotope ratio mass spectrometry (GC/Py/IRMS). Samples (in hexane) were injected into with a splitless injector at 250 °C with a flow rate of 1.2 mL/min. Separation was performed with a trace 1310 GC (Thermo Fischer Scientific GmbH, Bremen, Germany) equipped with a HP-5 capillary column (30 m × 0.25 mm, 0.25 μm film thickness). The GC oven temperature programs were as follows: 80 °C for 1 min, increased by 20 °C/min to 140 °C, held for 2 min, then by 5 °C/min to 280 °C and held for 6 min. After chromatographic separation, TCPP was thermally converted (pyrolyzed) in an Isolink conversion unit (Thermo Fischer Scientific GmbH, Bremen, Germany) to CO with a nonporous ceramic (Al_2O_3) tube operated at 1280 °C. The nonporous ceramic (Al_2O_3) tube (320 mm × 0.8 mm, 1.55 mm) was filled with a platinum tube with braided Ni-wires as catalyst. Isotope values of CO were determined with a MAT 253 plus IRMS (Thermo Fischer Scientific GmbH, Bremen, Germany). Before determination of $\delta^{18}O$ values of TCPP, the reproducibility and accuracy of the IRMS was evaluated with standard CO ($\delta^{18}O = -33.93$ ‰), and total uncertainty was about ± 0.2 ‰ (n = 6). All isotopic data obtained were first drift-corrected and then amount corrected following the procedure of Ma *et al.* and Zech and Glaser [33,34]. All reported isotope values were corrected to international reference standards by the International Atomic Energy Agency (IAEA, Vienna, Austria), IAEA-601 (benzoic acid, $\delta^{18}O_{V-SMOW} = +23.14$ ‰) for oxygen, and all $\delta^{18}O$ values remained within analytical uncertainty (± 0.2 ‰). More detailed information about isotope analysis is available in SI.

2.7. Quantum chemical calculations

To obtain more understanding about the transformation mechanisms of TCPP on a molecular scale, DFT based quantum chemical calculations focused on bond cleavage were performed with the Gaussian 09 package [35]. The geometry structure optimization algorithm using the M06–2X functional without any constraints in redundant internal coordinates optimized the geometry of reactants, complex compounds, and products [36]. The 6–31 + G(d,p) basis set was used for all elements. More detailed information about isotope analysis is available in SI.

3. Results and discussion

3.1. Degradation kinetics of TCPP

Prior to degradation experiments, preliminary experiments were performed under H_2O_2 only, UV only, and UV/H_2O_2 with a TCPP concentration of 1.0 mg/L. The hydrolysis experiments without UV and H_2O_2 as a control were carried out with a TCPP concentration of 1.0 mg/L. No significant removals of TCPP were observed in H_2O_2 only and UV only systems, while 98.2 % of TCPP was effectively removed with UV/H_2O_2 after 15 min (Fig. 1a). Due to the poor light absorbance properties of TCPP in the range of 200 nm $\leq \lambda \leq$ 800 nm (Fig. S1), the UV degradation of TCPP rarely occurs. In addition, no detectable hydrolysis occurred without UV and H_2O_2 after a week (Fig. 1d).

Degradation kinetics of TCPP with UV/H_2O_2 at various initial concentrations (C_0 ranging from 0.5 to 10 mg/L) are shown in Fig. 1b. TCPP of 0.5 and 1.0 mg/L were entirely degraded within about 12 and 15 min, respectively. Whereas, only 57.8 % of TCPP was degraded for 10 mg/L within 15 min. That is, the increase of initial concentration had a negative impact on the transformation rates. The reason may be that the ratio of available oxidizing species to TCPP concentration decreased with the increase of substrate concentration, resulting in the extension of transformation time. In addition, competitive action for oxidizing species between substrate and generated intermediates could occur as a result of increased intermediate formation at higher substrate concentrations [17,37].

Further, the impacts of H_2O_2 concentrations on the TCPP ($C_0 = 10$ mg/L) degradation efficiencies were explored. As clearly seen in Fig. 1c, an obvious promotion in the degradation of TCPP was observed with the H_2O_2 concentrations increased from 0.1 to 0.5 mg/L. However, when the H_2O_2 concentrations were higher than 0.5 mg/L, TCPP degradation efficiencies increased very slightly. As reported, organics can be degraded by $^\bullet OH$ generated from H_2O_2 in UV/H_2O_2 reaction system [17,38]. The reason may be that when H_2O_2 is present in excess, excess H_2O_2 can react with $^\bullet OH$ to form hydroperoxyl radical ($HO_2^\bullet$) [17]. The produced $HO_2^\bullet$ reacts with $^\bullet OH$ to consume the produced $^\bullet OH$ [37], subsequently stop the degradation of TCPP. Therefore, the transformation efficiencies of TCPP can be saturated because excess H_2O_2 can act as a scavenger of $^\bullet OH$.

3.2. Main ROSs during the degradation of TCPP

The degradation of TCPP occurred under H_2O_2 and UV irradiation. Generally, the degradation of organics in the ultraviolet and sunlight irradiation system may occur through indirect or sensitized photolysis reaction pathways. These pathways contain hydrogen abstraction, electron transfer, and formation of ROSs, involving reactions of ground state organics with other photochemically generated species [28]. The H_2O_2 and dissolved oxygen in aqueous phase can participate in the degradation of organic compounds by generating ROSs [39,40]. To detect the active species in ROSs-induced transformation of TCPP, the ROS initiators and scavengers were added to reaction solutions. The degradation of TCPP in the presence of TBA (10 mM) or MeOH (10 mM) under UV/H_2O_2 was examined (Fig. 2). It was clearly seen that 83.5 % and 51.9 % of TCPP degradation rates were suppressed in the reaction
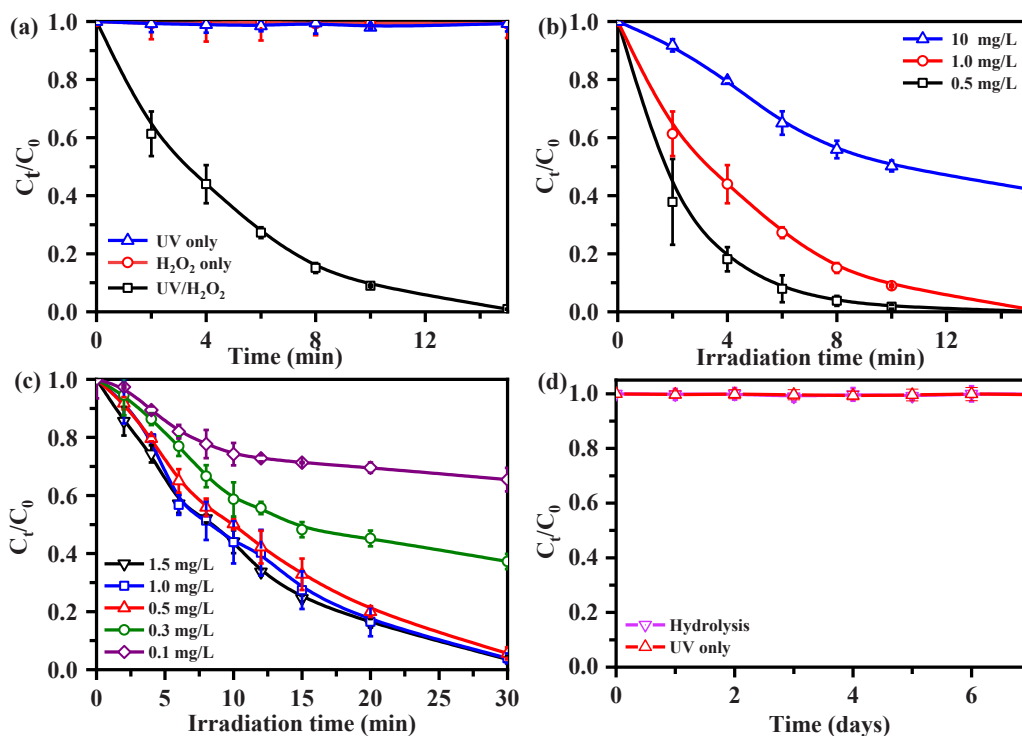
Fig. 1. (a) Comparison of TCPP ($C_0 = 1.0$ mg/L) degradation efficiencies under H_2O_2 only, UV only, and UV/H_2O_2; (b) Degradation of different TCPP concentrations under UV/H_2O_2 (0.5 mg/L); (c) Degradation of TCPP ($C_0 = 10$ mg/L) under different H_2O_2 concentrations with UV irradiation; (d) The hydrolysis control experiments of TCPP ($C_0 = 1.0$ mg/L) without UV/H_2O_2 after a week.
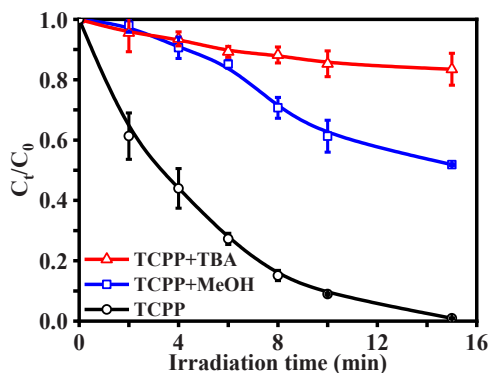

Fig. 2. Degradation of TCPP (1.0 mg/L) with H_2O_2 (0.5 mg/L) under UV irradiation (the red triangle represents the presence of tert-butanol (TBA) (10 mM), the blue square represents the presence of methanol (MeOH) (10 mM), and the black circle represents the absence of TBA and MeOH).

by adding TBA or MeOH as trapper of $^\bullet$OH within 15 min, respectively. The results double confirmed that TCPP degradation involve $^\bullet$OH in the UV/H_2O_2 system, although the suppressed degradation rates were different for TBA and MeOH. In TCPP solution without ROS trappers, $^\bullet$OH caused 99.1 % of TCPP degradation within 15 min.

To further clarify the main ROSs that could participate in the degradation of TCPP, the EPR spectra of TCPP aqueous solution with spin trapping agent were performed in UV/H_2O_2 system. DMPO was used for trapping $^\bullet$OH and $O_2^{\bullet-}$ [39,41], and TMPD was used for trapping $^1O_2$ [42]. Spin trapping of $^1O_2$ is established on the oxidation of diamagnetic TMPD by $^1O_2$ to form paramagnetic 2,2,6,6-tetramethyl-4--piperidone-1-oxyl (TMPD-O). As seen in Fig. 3a, a strong EPR signal consisting of four major signals with intensity ratio of 1:2:2:1 was observed with the increasing of microwave irradiation. This signal can be assigned as that from DMPO-OH. No signal of DMPO-$O_2^{\bullet-}$ was

observed. The intensity of DMPO-OH signal increased with the increase of microwave irradiation time. While no TMPD-O peak was detected in the presence of TMPD (Fig. 3b), which verified no formation of $^1O_2$ in this reaction system. These results double confirmed that $^\bullet$OH is the major ROSs generated in the UV/H_2O_2 reaction system.

3.3. Degradation intermediates of TCPP

The products of TCPP during the UV/H_2O_2 degradation process were further determined based on UPLC-Q exactive orbitrap-HRMS analysis and are shown in Table 1. Some intermediates could not be determined due to their low concentrations in the UV/H_2O_2 reaction mixtures. Total of nine photodegradation intermediates (B, C, D, E, F, G, H, I, and J with [M+H]$^+$ values of 250.9995, 343.0023, 309.0227, 174.9917, 266.9943, 340.9862, 307.0255, 323.0205, and 247.0134, respectively) were identified with positive mode. The intermediates were identified as keto, carbonylated and hydroxylated derivatives. Intermediates (B), (C), (E), (F), (G), (H), (I), and (J) had been observed for TCPP degradation in previous works [16,17]. Intermediate (D) was observed for the first time in our UV/H_2O_2 reaction system. From UPLC-Q exactive orbitrap-HRMS results of degradation intermediates, the chromatograms and detailed mass spectra of the degradation intermediates are provided in Figs. S2 and S3.

3.4. Stable isotope fractionations and degradation mechanisms

To elucidate the underlying degradation pathways of TCPP in UV/H_2O_2 reaction system, stable isotope analysis involving C, H and O was introduced. Isotope fractionations during the UV/H_2O_2 reaction process were measured based on C, H and O isotope compositions of TCPP at different intervals. The Rayleigh model was used to establish the relationship between the change of isotope composition and degree of degradation [43,44]. The resulting C and O isotope enrichment factors calculated according to Eqs. 2–4 are shown in Fig. 4. During the
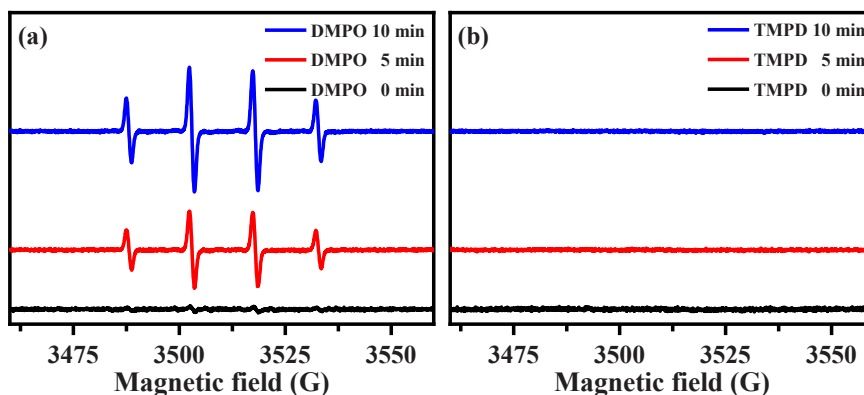
Fig. 3. EPR spectra generated in presence of H_2O_2 with (a) TCPP and DMPO for different periods of irradiation (0, 5, 10 min); (b) TCPP and TMPD for different periods of irradiation (0, 5, 10 min). EPR spectra were recorded at room temperature, using an EPR spectrometer, with 10 mW microwave irradiation (9.438 GHz) and 0.063 mT field modulation (100 kHz).

UV/H_2O_2 degradation of TCPP, C, H and O isotope shifted from −28.43 ‰ to −26.89 ‰, −88.83 ‰ to −90.61 ‰, and 28.62 ‰ to 25.64 ‰, respectively, at 57.8 % degradation rate efficiency. A normal C isotope effects (^{13}C-AKIEs = 1.0115 ± 0.0004, ε_C = −1.9 ± 0.4 ‰) along with significant inverse O isotope fractionation (^{18}O-AKIEs = 0.9897 ± 0.0005, ε_O = +2.6 ± 0.5 ‰) were observed during the UV/H_2O_2 reaction process. However, no H isotope fractionation was determined ($\Delta\delta^2$D ≤ ± 2.0 ‰).

The mechanistic scenarios for the occurrence of O isotope fractionation can be explained as follows. The anomalous inverse ε_O = 2.6 ± 0.5 ‰ was observed during the UV/H_2O_2 degradation of TCPP ($\Delta\delta^{18}$O = −2.98 ‰). Under UV irradiation, $^{\bullet}$OH generated by H_2O_2 had a high tendency to non-selective reaction on functional moieties of TCPP via hydrogen abstraction, electron transfer or electrophilic/radical addition [37]. The P-O or C-O bonds in TCPP can be broken by $^{\bullet}$OH, producing O isotope fractionation. To further elucidate the reaction mechanisms, the Gibbs free energy of P-O and C-O bond split was calculated with DFT. The results exhibited that the Gibbs free energy of C-O bond cleavage was 46.5 kcal/mol (Fig. 5, pink path), indicating that C-O bond cleavage was not likely to occur under the UV/H_2O_2 condition [45]. Similarly, the Gibbs free energy of P-O bond cleavage was 35.2 kcal/mol (Fig. 5, dark green path), also indicating that P-O bond cleavage was not possible. However, the Gibbs free energy of P-O bond cleavage through adduction of $^{\bullet}$OH to center phosphorus atom and then substitution of an oxygen-chlorinated isopropyl groups ($-OC_3H_6Cl$) was 17.9 kcal/mol (Fig. 5, black path), indicating that the reaction may occur through a two-step addition-elimination mechanism involving a penta-coordinate phosphoric intermediate. Therefore, combining the identified intermediates with DFT calculations, we can suggest that the rate-limiting step proceeds through an oxidative attack on the P = O bond by $^{\bullet}$OH to central phosphorus atom, generating a $(C_3H_6OCl)_3PO\cdot OH$ radicals. Then, the radicals were stabilized by elimination of the oxygen-chlorinated isopropyl groups ($-OC_3H_6Cl$) from phosphoric center. Zhao et al. [46] use oxygen isotope analysis to confirm the pathway of phosphate release during transformation of diazinon, an organophosphorus pesticide, in a Fe(III)-oxalate complex reaction system, and reveal that photodegradation of diazinon is initiated by breaking of P-O bonds. The P-O bonds in phosphates are resistant to inorganic hydrolysis, so the changes measured for oxygen isotope (^{18}O/^{16}O) can be used as a signature to characterize phosphonates from phosphor esters and organophosphorus [47]. Therefore, in this study, the observed oxygen isotope fractionation of TCPP highly supported a P-O bond split.

Meanwhile, a normal primary ε_C = -1.9 ± 0.4 ‰ was observed during the UV/H_2O_2 degradation of TCPP ($\Delta\delta^{13}$C = 1.5 ‰) (Fig. 4a). The cleavage of P-O bonds was not relevant to primary C isotope fractionation; thus, the C isotope fractionation cannot be attributed to the cleavage of P-O bonds. A previous study reported that the nucleophilic
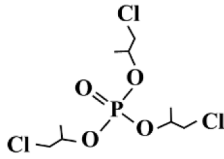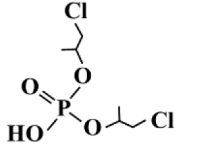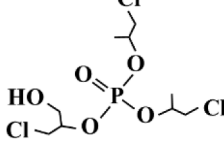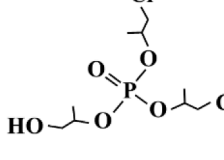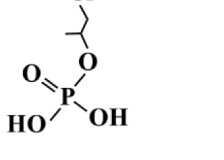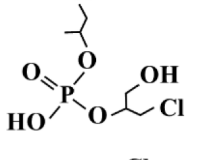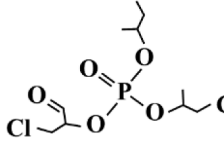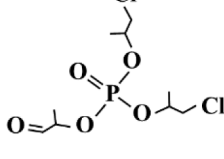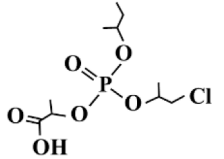
$^{\bullet}$OH-attack on phosphorus atoms of dichlorvos, an organophosphorus pesticide, led to P = S bond split without a primary C isotope effect, but a small value of ε_C (-0.2 ± 0.1 ‰) [26]. Considering that ε_C (-1.9 ± 0.4 ‰) in this study was higher than ε_C (-0.2 ± 0.1 ‰), other synergistic reactions might occur to lead to C isotope fractionation. Based on the UV/H_2O_2 transformation intermediates with analysis of conversion mechanisms, the C-H or C-Cl bond in TCPP can be broken to produce C isotope fractionation. In the UV/H_2O_2 system, $^{\bullet}$OH as nucleophilic reagent led to C-H bond cleavage via H abstraction of methyl group, and there may be associated with C isotope effects.

To confirm this pathway, the DFT was performed to calculate the Gibbs free energy of C-H bond cleavage. Results exhibited that the Gibbs free energy of C-H bond cleavage was 11.7 kcal/mol (Fig. 5, blue path), indicating that C-H bond cleavage can happen [45]. To further elucidate the reaction mechanisms, H isotope fractionation was measured during the UV/H_2O_2 transformation. If C-H bond cleavage is a rate-limiting step, the H abstraction reaction of methyl groups can be supposed to be accompanied by primary H isotope fractionation [44]. The negligible H isotope fractionation ($\Delta\delta^2$D ≤ ± 2.0 ‰ which is the confidence interval uncertainties) was observed in this study (Fig. 4c). Therefore, the breaking of C-H bond was not a rate-limiting step. In this study, the Gibbs free energy of C-Cl bond cleavage was 10.8 kcal/mol (Fig. 5, red path), showing that the breaking of C-Cl bonds was reasonable [45]. The primary C isotope fractionation indicated that the breaking of C-Cl bonds was a rate-limiting step and a typical mass-dependent carbon isotope fractionation, causing a regular AKIEs (enrichment of heavy isotope in remaining substrate, AKIEs > 1) for the atoms. The magnitude of the observed ^{13}C-AKIEs upon the UV/H_2O_2 degradation of TCPP in the present study was 1.0115. The obtained value was closed with the ^{13}C-AKIEs (1.0126 − 1.0234) reported by Zakon et al. [48] for UV debromination of brominated phenols, and the ^{13}C-AKIEs of around 1.03 reported by Zwank et al. [49] for the reductive dechlorination of tetrachloromethane. Therefore, $^{\bullet}$OH radicals as nucleophilic reagents attacked on C-Cl bonds involving a heterolytic cleavage of C-Cl bonds and C isotope fractionation during the UV/H_2O_2 degradation.

Based on the isotope analysis and intermediate identification, three underlying pathways could be deduced during the UV/H_2O_2 degradation of TCPP (Scheme 1). Pathway I, $^{\bullet}$OH was adduction to the center phosphorus atom, forming a $(C_3H_6OCl)_3PO\cdot OH$ radical (A1) (Scheme 1, Rout I). Subsequently, the oxygen-chlorinated isopropyl group ($-OC_3H_6Cl$) may be substituted by $^{\bullet}$OH to produce compound bis(1-chloro-2-propyl) phosphate (B). Similar pathway has been observed previously for the $^{\bullet}$OH attack on the tris(2-chloroethy) phosphate, tributyl phosphate [27], and dimethyl phenylphosphonate [50]. Furthermore, bis(1-chloro-2-propyl) phosphate involved $^{\bullet}$OH substitution to form 1-chloropropan-2-yl dihydrogen phosphate (E) and H-abstraction of methyl group by $^{\bullet}$OH to form
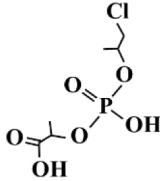
Table 1

Summary of Intermediates Identified by UPLC-Q Exactive Orbitrap-HRMS (The Initial Concentration of TCPP was 10 mg/L).

No.	Compounds	Rt/min	Observed m/z	Formula	Structure formula
A	tris(1-chloro−2-propyl) phosphate	20.42	327.0021	$C_9H_{18}Cl_3O_4P$	
B	bis(1-chloro−2-propyl) phosphate	5.27	250.9995	$C_6H_{13}Cl_2O_4P$	
C	1-chloro−3-hydroxypropan−2-yl bis(1-chloropropan−2-yl) phosphate	13.10	343.0023	$C_9H_{18}Cl_3O_5P$	
D	bis(1-chloropropan−2-yl) (1-hydroxypropan−2-yl) phosphate	10.13	309.0227	$C_9H_{19}Cl_2O_5P$	
E	1-chloropropan−2-yl dihydrogen phosphate	1.90	174.9917	$C_3H_8ClO_4P$	
F	1-chloro−3-hydroxypropan−2-yl (1-chloropropan−2-yl) hydrogen phosphate	3.20	266.9943	$C_6H_{13}Cl_2O_5P$	
G	1-chloro−3-oxopropan−2-yl bis(1-chloropropan−2-yl) phosphate	11.86	340.9862	$C_9H_{16}Cl_3O_5P$	
H	bis(1-chloropropan−2-yl) (1-oxopropan−2-yl) phosphate	9.94	307.0255	$C_9H_{17}Cl_2O_5P$	
I	2-((bis((1-chloropropan−2-yl)oxy)phosphoryl)oxy)propanoic acid	11.45	323.0205	$C_9H_{17}Cl_2O_6P$	

(*continued on next page*)

Table 1 (*continued*)

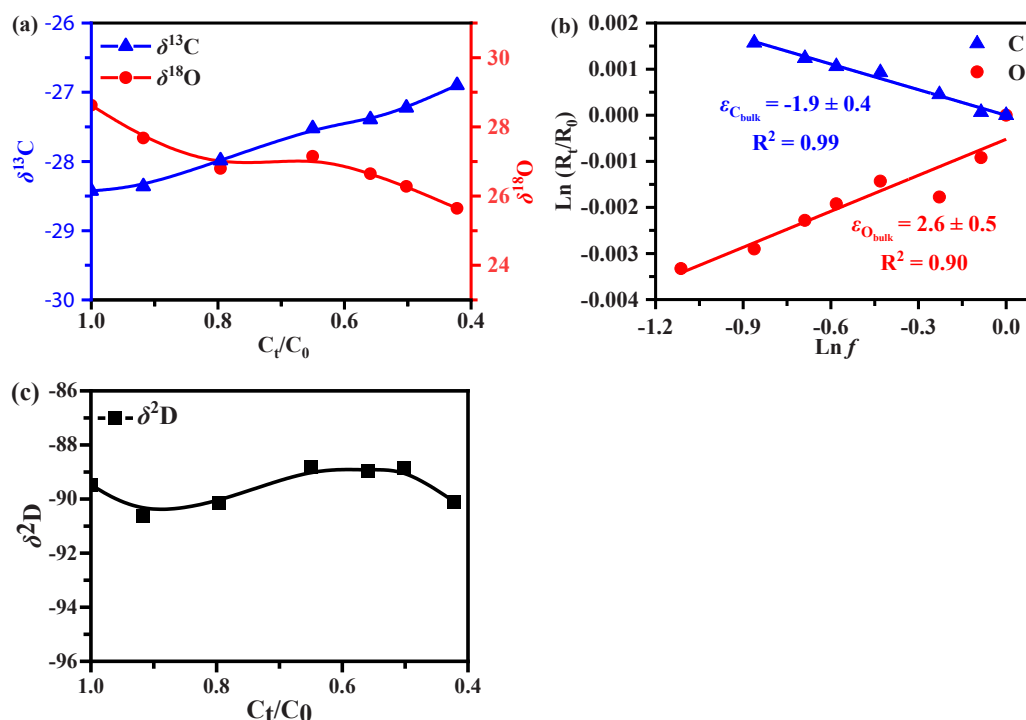| No.	Compounds	Rt/min	Observed m/z	Formula	Structure formula
J	2-((((1-chloropropan−2-yl)oxy)(hydroxy)phosphoryl)oxy)propanoic acid	2.12	247.0134	$C_6H_{12}ClO_6P$	

Fig. 4. Isotope fractionations of TCPP during the UV/H_2O_2 reaction process. (a) showed the evolution of $\delta^{13}C$ and $\delta^{18}O$ values *vs* remaining fraction of TCPP. (b) showed the linearized isotope enrichment used to derive enrichment factors in eq. 2. (c) showed the evolution of δ^2H values *vs* remaining fraction of TCPP.

1-chloro-3-hydroxypropan-2-yl (1-chloropropan-2-yl) hydrogen phosphate (F). Pathway II, hydrogen abstraction from the methyl-C position of oxygen-chlorinated isopropyl arm by $^\bullet$OH formed a carbon centered radical $^\bullet C_9H_{17}Cl_3O_4P$ (A2), which was followed by oxygen addition to generate the peroxyl radical $^\bullet C_9H_{17}Cl_3O_6P$ (A3). Peroxyl radicals typically undergo a bimolecular Russell mechanism [51] leading to the corresponding hydroxylated 1-chloro-3-hydroxypropan-2-yl bis (1-chloropropan-2-yl) phosphate (C) (Scheme 1, Rout II). Previous studies showed that hydrogen abstraction was the main mechanism for photocatalytic oxidation of dimethyl methyl phosphonate through $^\bullet$OH attack [52] and tris(2-chloroethyl) phosphate through persulfate radical attack [53]. No significant hydrogen isotope fractionation was observed during hydrogen abstraction reaction in this study, demonstrating that H-bond split was not the rate-limiting step. Combination of negligible hydrogen isotope fractionation and the number of intermediates from hydrogen abstraction reaction of TCPP indicated that hydrogen abstraction reaction pathway was not the main pathway. The subsequent reaction of hydroxylated tris(1-chloro-2-propyl) phosphate (C) may be oxidized to form the corresponding ketone 1-chloro-3-oxopropan-2-yl bis(1-chloropropan-2-yl) phosphate (G). Pathway III involved the attacking of C-Cl bond by $^\bullet$OH to form hydroxylated derivative bis (1-chloropropan-2-yl) (1-hydroxypropan-2-yl) phosphate (D) (Scheme 1, Rout III). Significant carbon isotope fractionation was observed

during C-Cl bond split, demonstrating that C-Cl bond split was the rate-limiting step of the $^\bullet$OH addition. In subsequent step, hydroxyl groups undergo oxidation reaction by $^\bullet$OH leading to corresponding aldehyde bis(1-chloropropan-2-yl) (1-oxopropan-2-yl) phosphate (H), and carboxylic acid 2-((bis((1-chloropropan-2-yl)oxy)phosphoryl)oxy) propanoic acid (I). Furthermore, the corresponding hydroxyl compound 2-((((1-chloropropan-2-yl)oxy)(hydroxy)phosphoryl)oxy)propanoic acid (I) was generated after substitution of 2-((bis((1-chloropropan-2-yl) oxy)phosphoryl)oxy) propanoic acid (I) by $^\bullet$OH. Generally, TCPP can be transformed to PO_4^{3-}, Cl^- and all kinds of intermediates through different degradation routes and the major reaction mechanisms include oxidation, dichlorination and dealkylation.

4. Conclusions

This research explored the kinetics and mechanisms of TCPP degradation by UV/H_2O_2, and a special attention was focused on stable isotope fractionation of C, H and O. TCPP can be efficiently degraded during the UV/H_2O_2 process, and the $^\bullet$OH radicals were verified to be predominant ROSs in the UV/H_2O_2 degradation system. Intermediates analysis showed that TCPP was transformed into a series of hydroxylated and dechlorinated intermediates. The C, H and O isotope fractionations were used diagnostically to characterize the UV/H_2O_2
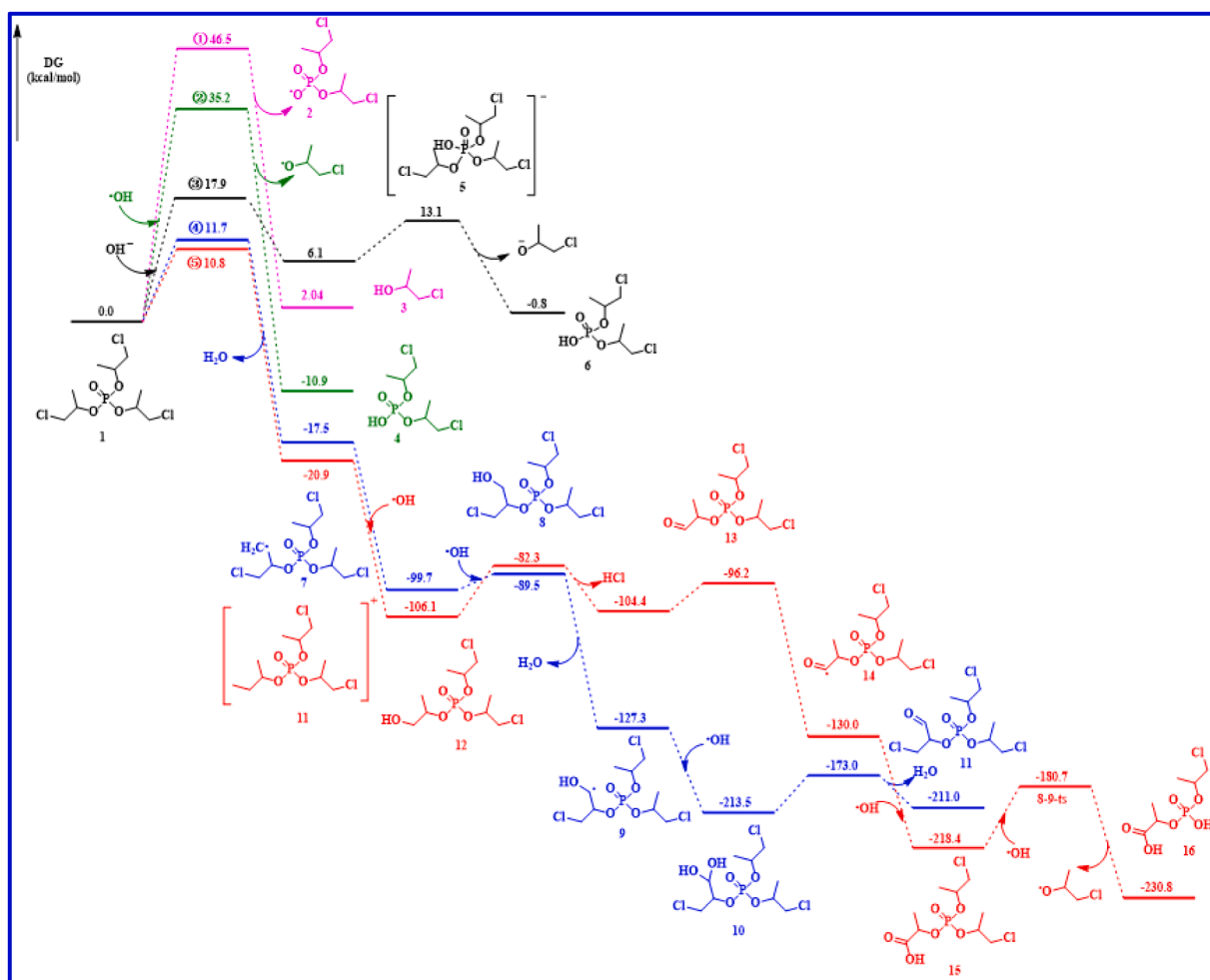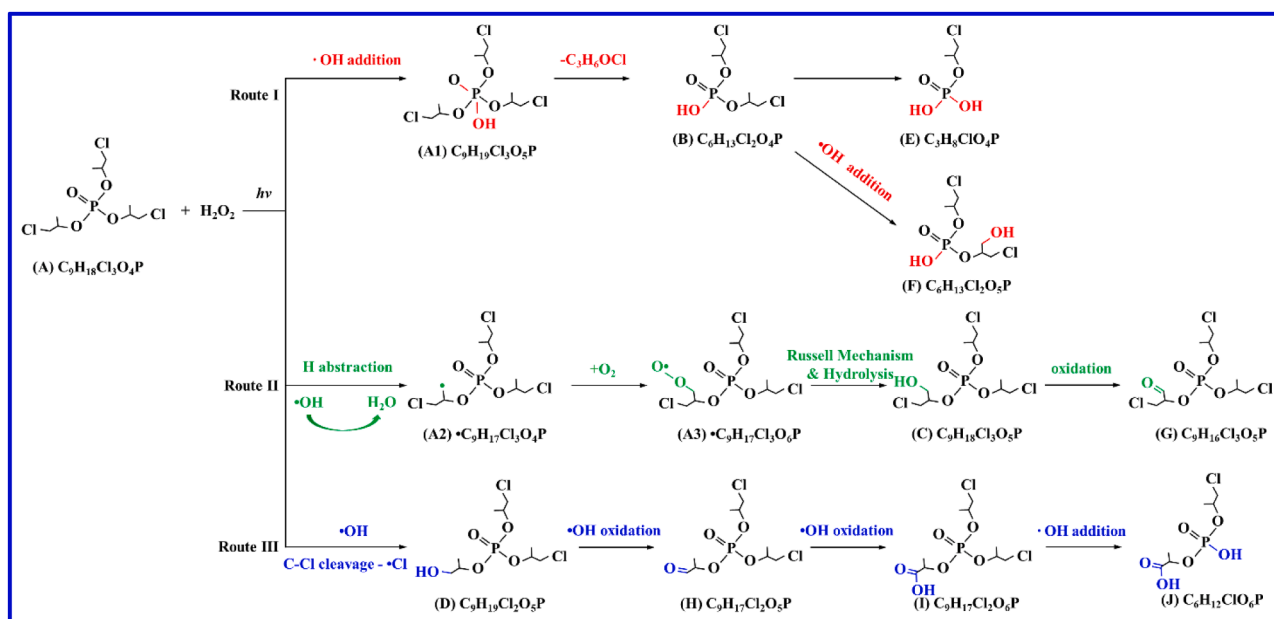
Fig. 5. The transition states of TCPP during UV/H$_2$O$_2$ degradation process.

Scheme 1. Proposed transformation mechanisms of TCPP in the UV/H$_2$O$_2$ system.

degradation pathways of TCPP. Large O isotope fractionation combined with the DFT calculations indicated that the degradation of TCPP in the UV/H_2O_2 reaction system initiated by P-O bond cleavage and the breaking of P-O bond was the rate-limiting step. Remarkable C isotope fractionation and no significant H stable isotope fractionation in this system indicated that C-Cl bond rather than C-H bond breaking was the rate-limiting step. These results demonstrated that the characteristic isotope fractionation upon UV/H_2O_2 degradation of TCPP may be used for exploring predominant degradation pathways. The UV/H_2O_2 degradation was considered to be the main transformation pathways for organophosphorus flame retardants. These systematic studies on the C, H and O isotope fractionation of organophosphorus flame retardants showed the potential of applying the isotope fraction to analyze chemical reactions in the aqueous environments. To further explore the diagnostic potential of tracing degradation mechanisms in the environments applying isotope fractionation, systematic research on microbial transformation was required and C, H and O isotope fractionation need to be compared with those of chemical transformation reactions.

CRediT authorship contribution statement

Guo Yi: Validation, Methodology, Investigation. **Chen Suyun:** Formal analysis, Data curation. **Xiong Jukun:** Writing – original draft, Methodology, Formal analysis, Data curation. **An Taicheng:** Writing – review & editing, Supervision, Conceptualization. **Wen Meicheng:** Validation, Methodology. **Gao Yanpeng:** Validation, Methodology. **Li Guiying:** Writing – review & editing, Validation. **Gelman Faina:** Writing – review & editing, Validation, Methodology. **Wang Zicong:** Validation, Methodology.

Declaration of Competing Interest

The authors declare that they have no known competing financial interests or personal relationships that could have appeared to influence the work reported in this paper.

Appendix A. Supporting information

Supplementary data associated with this article can be found in the online version at doi:10.1016/j.jece.2025.116223.

Data availability

No data was used for the research described in the article.

References

[1] T.B. Chokwe, O.A. Abafe, S.P. Mbelu, J.O. Okonkwo, L.L. Sibali, A review of sources, fate, levels, toxicity, exposure and transformations of organophosphorus flame-retardants and plasticizers in the environment, Emerg. Contam. 6 (2020) 345–366.

[2] C. Liang, Y. He, X.J. Mo, H.X. Guan, L.Y. Liu, Universal occurrence of organophosphate tri-esters and di-esters in marine sediments: Evidence from the Okinawa Trough in the East China Sea, Environ. Res. 248 (2024) 118308.

[3] ECHA, Authorization list. Online, Accessed 13 March 2020). European chemicals agency, 2018, ⟨https://echa.europa.eu/authorisation-list⟩. Accessed 13 March 2020).

[4] Q. Zhang, Y. Wang, C. Zhang, Y. Yao, L. Wang, H. Sun, A review of organophosphate esters in soil: Implications for the potential source, transfer, and transformation mechanism, Environ. Res. 204 (2022) 112122.

[5] S.C. Hammel, H.M. Stapleton, B. Eichner, K. Hoffman, Reconsidering an appropriate urinary biomarker for flame retardant tris(1-chloro-2-propyl)

[6] Y. Vasseghian, M. Alimohamadi, A. Khataee, E.N. Dragoi, A global systematic review on the concentration of organophosphate esters in water resources: Meta-analysis, and probabilistic risk assessment, Sci. Total Environ. 807 (2022) 150876.

[7] X. Guan, G. Zhang, L. Meng, M. Liu, L. Zhang, C. Zhao, Y. Li, Q. Zhang, G. Jiang, Novel biomonitoring method for determining five classes of legacy and alternative flame retardants in human serum samples, J. Environ. Sci. 131 (2023) 111–122.

[8] T. Xu, P. Li, S. Wu, L. Lei, D. He, Tris(2-chloroethyl) phosphate (TCEP) and tris(2-chloropropyl) phosphate (TCPP) induce locomotor deficits and dopaminergic degeneration in Caenorhabditis elegans, Toxicol. Res. 6 (2017) 63–72.

[9] Z. Percy, A. Chen, W. Yang, J.M. Braun, B. Lanphear, M. Ospina, A.M. Calafat, C. Xie, K.M. Cecil, A.M. Vuong, Y. Xu, K. Yolton, Childhood urinary organophosphate esters and cognitive abilities in a longitudinal cohort study, Environ. Res. 215 (2022) 114265.

[10] E. Commission, European Commission, Regulation (EC) No. 2364/2000 of 25 October 2000 Concerning the fourth list of priority substances as foreseen under council regulation (EEC) No. 793/3, 2000, European Chemicals Bureau: Ispqra, Italy, 2000.

[11] X. Zhu, S. Deng, Y. Fang, S. Yang, Y. Zhong, D. Li, H. Wang, J. Wu, P.A. Peng, Dehalococcoides-containing enrichment cultures transform two chlorinated organophosphate esters, Environ. Sci. Technol. 56 (2022) 1951–1962.

[12] H. He, Q. Ji, Z. Gao, S. Yang, C. Sun, S. Li, L. Zhang, Degradation of tri(2-chloroisopropyl) phosphate by the UV/H_2O_2 system: Kinetics, mechanisms and toxicity evaluation, Chemosphere 236 (2019) 124388.

[13] X. Yu, H. Yin, H. Peng, G. Lu, Z. Liu, H. Li, Z. Dang, Degradation mechanism, intermediates and toxicology assessment of tris-(2-chloroisopropyl) phosphate using ultraviolet activated hydrogen peroxide, Chemosphere 241 (2020) 124991.

[14] J. Ye, S. Tang, R. Qiu, S. Chen, H. Liu, Biodegradation pathway and mechanism of tri (2-chloropropyl) phosphate by Providencia rettgeri, J. Environ. Sci. 144 (2024) 26–34.

[15] M. Antonopoulou, P. Karagianni, I.K. Konstantinou, Kinetic and mechanistic study of photocatalytic degradation of flame retardant Tris (1-chloro-2-propyl) phosphate (TCPP), Appl. Catal. B-Environ. 192 (2016) 152–160.

[16] X. Yu, H. Yin, J.S. Ye, H. Peng, G. Lu, Z. Dang, Degradation of tris-(2-chloroisopropyl) phosphate via UV/TiO_2 photocatalysis: kinetic, pathway, and security risk assessment of degradation intermediates using proteomic analyses, Chem. Eng. J. 374 (2019) 263–273.

[17] Y. Son, Y.M. Lee, K.D. Zoh, Kinetics and degradation mechanism of tris (1-chloro-2-propyl) phosphate in the UV/H_2O_2 reaction, Chemosphere 260 (2020) 127461.

[18] P. Alvarez-Zaldivar, S. Payraudeau, F. Meite, J. Masbou, G. Imfeld, Pesticide degradation and export losses at the catchment scale: Insights from compound-specific isotope analysis (CSIA), Water Res 139 (2018) 198–207.

[19] B. Shi, J. Meng, T. Wang, Q. Li, Q. Zhang, G. Su, The main strategies for soil pollution apportionment: A review of the numerical methods, J. Environ. Sci. 136 (2024) 95–109.

[20] B.A. Asfaw, K. Sakaguchi-Soeder, T. Schiedek, N. Michelsen, A. Bernstein, H. Siebner, C. Schueth, Isotopic evidence (δ^{13}C, δ^{37}Cl, δ^2H) for distinct transformation mechanisms of chloroform: Catalyzed H_2-water system vs. zero-valent iron (ZVI), J. Environ. Chem. Eng. 11 (2023) 110005.

[21] M. Ratti, S. Canonica, K. McNeill, P.R. Erickson, J. Bolotin, T.B. Hofstetter, Isotope fractionation associated with the direct photolysis of 4-chloroaniline, Environ. Sci. Technol. 49 (2015) 4263–4273.

[22] S. Lian, L. Wu, M. Nikolausz, O.J. Lechtenfeld, H.H. Richnow, ^{2}H and ^{13}C isotope fractionation analysis of organophosphorus compounds for characterizing transformation reactions in biogas slurry: Potential for anaerobic treatment of contaminated biomass, Water Res. 163 (2019) 114882.

[23] L. Melander, W.H. Saunders, John Wiley & Sons. Reaction rates of isotopic molecules, Wiley Interscience Publication, 1980, p. 331.

[24] L. Wu, D. Verma, M. Bondgaard, A. Melvej, C. Vogt, S. Subudhi, H.H. Richnow, Carbon and hydrogen isotope analysis of parathion for characterizing its natural attenuation by hydrolysis at a contaminated site, Water Res 143 (2018) 146–154.

[25] L. Wu, J. Yao, P. Trebse, N. Zhang, H.H. Richnow, Compound specific isotope analysis of organophosphorus pesticides, Chemosphere 111 (2014) 458–463.

[26] L. Wu, B. Chládková, O.J. Lechtenfeld, S. Lian, J. Schindelka, H. Herrmann, H. H. Richnow, Characterizing chemical transformation of organophosphorus compounds by ^{13}C and ^{2}H stable isotope analysis, Sci. Total Environ. 615 (2018) 20–28.

[27] J. Liu, L. Wu, S. Kuemmel, J. Yao, T. Schaefer, H. Herrmann, H.H. Richnow, Carbon and hydrogen stable isotope analysis for characterizing the chemical degradation of tributyl phosphate, Chemosphere 212 (2018) 133–142.

[28] H. Fang, Y. Gao, G. Li, J. An, P.-K. Wong, H. Fu, S. Yao, X. Nie, T. An, Advanced oxidation kinetics and mechanism of preservative propylparaben degradation in aqueous suspension of TiO_2 and risk assessment of Its degradation products, Environ. Sci. Technol. 47 (2013) 2704–2712.

[29] D.R. Duling, Simulation of multiple isotropic spin-trap EPR spectra, J. Magn. Reson. Ser. B 104 (1994) 105–110.

[30] J. Xiong, G. Li, P.A. Peng, F. Gelman, Z. Ronen, T. An, Mechanism investigation and stable isotope change during photochemical degradation of tetrabromobisphenol A (TBBPA) in water under LED white light irradiation, Chemosphere 258 (2020) 127378.

[31] J. Renpenning, S. Kümmel, K.L. Hitzfeld, A. Schimmelmann, M. Gehre, Compound-specific hydrogen isotope analysis of heteroatom-bearing compounds via gas chromatography–chromium-based high-temperature conversion (Cr/HTC)–isotope ratio mass spectrometry, Anal. Chem. 87 (2015) 9443–9450.

[32] J. Renpenning, A. Schimmelmann, M. Gehre, Compound-specific hydrogen isotope analysis of fluorine-, chlorine-, bromine- and iodine-bearing organics using gas chromatography-chromium-based high-temperature conversion (Cr/HTC) isotope ratio mass spectrometry, Rapid Commun. Mass Sp. 31 (2017) 1095–1102.

[33] R. Ma, Z. Zhu, B. Wang, Y. Zhao, X. Yin, F. Lu, Y. Wang, J. Su, C.H. Hocart, Y. Zhou, Novel position-specific O-18/O-16 measurement of carbohydrates. I. O-3 of glucose and confirmation of O-18/O-16 heterogeneity at natural abundance levels in glucose from starch in a C-4 plant, Anal. Chem. 90 (2018) 10293–10301.

[34] M. Zech, B. Glaser, Compound-specific delta O-18 analyses of neutral sugars in soils using gas chromatography-pyrolysis-isotope ratio mass spectrometry: problems, possible solutions and a first application, Rapid Commun. Mass Sp. 23 (2009) 3522–3532.

[35] M.J.T. Frisch, G.W.; Schlegel, H.B.; Scuseria, G.E.; Robb, M.A.; Cheeseman, J.R.; Scalmani, G.; Barone, V.; Mennucci, B.; Petersson, G.A.; Nakatsuji, H.; Caricato, M.; Li, X.; Hratchian, H.P.; Izmaylov, A.F.; Bloino, J.; Zheng, G.; Sonnenberg, J.L.; Hada, M.; Ehara, M.; Toyota, K.; Fukuda, R.; Hasegawa, J.; Ishida, M.; Nakajima, T.; Honda, Y.; Kitao, O.; Nakai, H.; Vreven, T.; MontGomery, J.A., Jr.; Peralta, J.E.; Ogliaro, F.; Bearpark, M.; Heyd, J.J.; Brothers, E.; Kudin, K.N.; Staroverov, V.N.; Kobayashi, R.; Normand, J.; Raghavachari, K.; Rendell, A.; Burant, J.C.; Iyengar, S. S.; Tomasi, J.; Cossi, M.; Rega, N.; Millam, J.M.; Klene, M.; Knox, J.E.; Cross, J.B.; Bakken, V.; Adamo, C.; Jaramillo, J.; Gomperts, R.; Stratmann, R.E.; Yazyev, O.; Austin, A.J.; Cammi, R.; Pomelli, C.; Ochterski, J.W.; Martin, R.L.; Morokuma, K.; Zakrzewski, V.G.; Voth, G.A.; Salvador, P.; Dannenberg, J.J.; Dapprich, S.; Daniels, A.D.; Farkas, O.; Foresman, J.B.; Ortiz, J.V.; Cioslowski, J.; Fox, D.J., Gaussian 09, Gaussian, Inc.: Wallingford CT, (2009).

[36] Y. Zhao, D.G. Truhlar, The M06 suite of density functionals for main group thermochemistry, thermochemical kinetics, noncovalent interactions, excited states, and transition elements: two new functionals and systematic testing of four M06-class functionals and 12 other functionals, Theor. Chem. Acc. 120 (2008) 215–241.

[37] G.V. Buxton, C.L. Greenstock, W.P. Helman, A.B. Ross, Critical review of rate constants for reactions of hydrated electrons, hydrogen atoms and hydroxyl radicals ($\bullet$OH/$\bullet$O-) in aqueous solution, J. Phys. Chem. Ref. Data 17 (1988) 513–886.

[38] Q. Ji, D. Sun, S. Yang, H. He, Z. Gao, C. Sun, S. Li, L. Zhang, Oxidation degradation of tri(dichloropropyl) phosphate by UV/H_2O_2 system: Degradation pathways and risk assessment of intermediates, J. Environ. Chem. Eng. 8 (2020) 104513.

[39] Y. Chen, C. Hu, J. Qu, M. Yang, Photodegradation of tetracycline and formation of reactive oxygen species in aqueous tetracycline solution under simulated sunlight irradiation, J. Photochem. Photobio. A-Chem. 197 (2008) 81–87.

[40] X. Wang, X. Hu, H. Zhang, F. Chang, Y. Luo, Photolysis kinetics, mechanisms, and pathways of tetrabromobisphenol A in water under simulated solar light irradiation, Environ. Sci. Technol. 49 (2015) 6683–6690.

[41] Y. Bao, J. Niu, Photochemical transformation of tetrabromobisphenol A under simulated sunlight irradiation: Kinetics, mechanism and influencing factors, Chemosphere 134 (2015) 550–556.

[42] Q. Zhu, M. Igarashi, M. Sasaki, T. Miyamoto, R. Kodama, M. Fukushima, Degradation and debromination of bromophenols using a free-base porphyrin and metalloporphyrins as photosensitizers under conditions of visible light irradiation in the absence and presence of humic substances, Appl. Catal. B-Environ. 183 (2016) 61–68.

[43] A.E. Hartenbach, T.B. Hofstetter, P.R. Tentscher, S. Canonica, M. Berg, R. P. Schwarzenbach, Carbon, hydrogen, and nitrogen isotope fractionation during light-induced transformations of atrazine, Environ. Sci. Technol. 42 (2008) 7751–7756.

[44] M. Elsner, L. Zwank, D. Hunkeler, R.P. Schwarzenbach, A new concept linking observable stable isotope fractionation to transformation pathways of organic pollutants, Environ. Sci. Technol. 39 (2005) 6896–6916.

[45] L. Gorb, J. Leszczynski, Intramolecular proton transfer in mono- and dihydrated tautomers of guanine: An ab initio post *Hartree-Fock* study, J. Am. Chem. Soc. 120 (1998) 5024–5032.

[46] J. Zhao, Y. Jiang, M. Kong, G. Liu, D.D. Dionysiou, Fe(III)-oxalate complex mediated phosphate released from diazinon photodegradation: Pathway signatures based on oxygen isotopes, J. Hazard. Mater. 358 (2018) 319–326.

[47] G. Cui, G. Lartey-Young, C. Chen, L. Ma, Photodegradation of pesticides using compound-specific isotope analysis (CSIA): a review, Rsc Adv. 11 (2021) 25122–25140.

[48] Y. Zakon, L. Halicz, F. Gelman, Bromine and carbon isotope effects during photolysis of brominated phenols, Environ. Sci. Technol. 47 (2013) 14147–14153.

[49] L. Zwank, M. Elsner, A. Aeberhard, R.P. Schwarzenbach, S.B. Haderlein, Carbon isotope fractionation in the reductive dehalogenation of carbon tetrachloride at iron (hydr)oxide and iron sulfide minerals, Environ. Sci. Technol. 39 (2005) 5634–5641.

[50] Y.C. Oh, Y. Bao, W.S. Jenks, Isotope studies of photocatalysis TiO$_2$-mediated degradation of dimethyl phenylphosphonate, J. Photochem. Photobio. A-Chem. 161 (2003) 69–77.

[51] S. Miyamoto, G.R. Martinez, M.H.G. Medeiros, P.Di Mascio, Singlet molecular oxygen generated from lipid hydroperoxides by the Russell mechanism:: Studies using ^{18}O-labeled linoleic acid hydroperoxide and monomol light emission measurements, J. Am. Chem. Soc. 125 (2003) 6172–6179.

[52] A. Aguila, K.E.O. Shea, T. Tobien, K.D. Asmus, Reactions of hydroxyl radical with dimethyl methylphosphonate and diethyl methylphosphonate. A fundamental mechanistic study, J. Phys. Chem. A 105 (2001) 7834–7839.

[53] H.S. Ou, J. Liu, J.S. Ye, L.L. Wang, N.Y. Gao, J. Ke, Degradation of tris(2-chloroethyl) phosphate by ultraviolet-persulfate: Kinetics, pathway and intermediate impact on proteome of Escherichia coli, Chem. Eng. J. 308 (2017) 386–395.